# Structural basis of actin filament capping at the barbed-end: a cryo-electron microscopy study

## Akihiro Narita[1,2], Shuichi Takeda[1,2], Atsuko Yamashita[2,4] and Yuichiro Maéda[1,2,3,*]

[1]ERATO Actin Filament Dynamics Project, Japan Science and Technology Agency, c/o RIKEN, Sayo, Hyogo, Japan, [2]Laboratory for Structural Biochemistry, RIKEN Harima Institute SPring-8 Center, Sayo, Hyogo, Japan and [3]Division of Biological Science, Graduate School of Science, Nagoya University, Furo-cho, Nagoya, Japan

The intracellular distribution and migration of many protein complexes and organelles is regulated by the dynamics of the actin filament. Many actin filament end-binding proteins play crucial roles in actin dynamics, since polymerization and depolymerization of actin protomers occur only at the filament ends. We present here an EM structure of the complex of the actin filament and hetero-dimeric capping protein (CP) bound to the barbed-end at 23 Å resolution, by applying a newly developed methods of image analysis to cryo-electron micrographs. This structure was fitted by the crystal structure of CP and the proposed actin filament structure, allowing us to construct a model that depicts two major binding regions between CP and the barbed-end. This binding scheme accounted for the results of newly performed and previously published mutation experiments, and led us to propose a two-step binding model. This is the first determination of an actin filament end structure.

## Introduction

Actin is one of the most abundant proteins in eukaryotic cells. Actin forms a double-stranded helical filament with a clear polarity; the polymerization and depolymerization at one end (barbed-end) is much faster than the other end (pointed-end). The actin filament plays cellular roles through its dynamic properties. Especially several types of motility is driven by polymerization and depolymerization (the actin dynamics) (Pantaloni *et al*, 2001; Pollard and Borisy, 2003). Capping protein (CP) binds to the barbed-end of the actin filament with a high affinity ($K_d \sim 1$ nM) and a 1:1 stoichiometry (Isenberg *et al*, 1980; Caldwell *et al*, 1989a; Schafer

*Corresponding author. ERATO Actin Filament Dynamics Project, Japan Science and Technology Agency, c/o RIKEN, Harima SPring-8 Center, 1-1-1 Kouto, Sayo, Hyogo 679-5148, Japan. Tel.: +81 791 58 2822; Fax: +81 791 58 2836; E-mail: ymaeda@spring8.or.jp
[4]Present address: Molecular Signaling Research Team, Structural Physiology Research Group, RIKEN Harima Institute SPring-8 Center, Sayo, Hyogo 679-5148, Japan

*et al*, 1993; Wear and Cooper, 2004), thus preventing the addition and loss of actin monomers at the end. CP is indispensable for the actin dynamics; the absence of CP prevented the reconstitution of the motility of *Listeria* and *Shigella in vitro* (Loisel *et al*, 1999). CP (CapZ in muscle) stabilizes and targets the actin filament in muscle (Casella *et al*, 1987; Schafer *et al*, 1993). Based on the crystal structure of CP (Yamashita *et al*, 2003), we previously proposed 'the tentacle binding mechanism', in which the C-terminus regions (α- and β-tentacle) of both CP subunits (α and β) extended from the rest of CP (the main body of CP) are crucial for its binding to the actin filament end. In the present work, we obtained an electron microscope (EM) structure of the actin–CP complex, which indicated that the α-tentacle must lie extended on the surface of CP, and together with a part of the CP body, displaying the cluster of basic residues. The basic residues must interact with acidic residues on the two end actin protomers simultaneously. The β-tentacle, seen as a freely mobile α-helix in the crystal, may be lifted up to exert hydrophobic interactions with the end protomer. The actin–CP complex structure, together with previous results, led us to propose an intriguing two-step binding mechanism by which the fluctuating actin filament end is capped by CP.
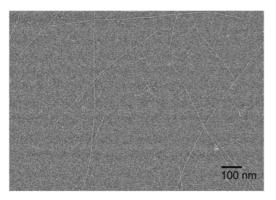
## Results

### Overview of the actin–CP structure

Cryo-electron micrographs of the actin–CP complex (Figure 1) were collected and processed by the use of novel procedures, which are described in full detail elsewhere (Narita and Maéda, 2006 and Materials and methods). This method is based on single particle analysis, and, among various methods for structural biology, this is the first for determining actin filament end structures. For the actin–CP complex, the resolution was evaluated as 23.3 Å (Figure 2). In the electron density map thus obtained (Figure 3A–F), individual masses are clearly recognized as actin protomers, except for the bottom mass that is clearly distinct from the rest, for it is more elongated and has a triangle-shaped protrusion on its bottom. This end mass contacts with two masses of actin protomers and fits very well with the crystal structure of CP (Yamashita *et al*, 2003), except for some small protruding loops and the β-tentacle (see below). The remaining masses follow the canonical actin helix up to the end and fit with the atomic structure of the actin filament (Lorenz *et al*, 1993) (Figure 3G and I). The orientation of CP was also unambiguously identified; as indicated in Figure 3G, the edge (orange arrow) on the left-hand side is longer than that on the right (red arrow), indicating that the α-subunit is on the left side and the β-subunit is on the right side, when the complex is viewed as in Figure 3G.
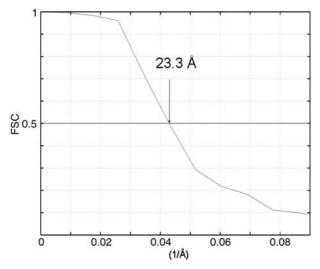
### Actin–CP binding interface

Based on the fitted atomic models, amino-acid residues involved at the interface between the actin filament and the

**Figure 1** A cryo-electron micrograph of the actin–CP complex. This is a digitized micrograph after CTF phase correction was made. Therefore, proteins are seen in bright contrast.



**Figure 2** Evaluation of the resolution of the obtained 3D electron density map (Frank, 2002). We divided the images of the actin–CP complex into two groups and reconstructed two 3D maps, which were compared by Fourier Shell Correlation (van Heel, 1987). The resolution was estimated as 23.3 Å, with a threshold of 0.5.

CP were predicted (Figure 4). Below, an actin filament is presented with the barbed-end down, and the actin protomer at the bottom and the one above it are referred to as protomers B and B-1, respectively (Figure 4A). On CP, the interface is formed by the α-tentacle and part of the surface composed of both CP subunits. The α-tentacle (shown in yellow in Figure 4A and B) interacts with the inner surface (the surface that faces the filament axis) of actin protomer B, including the hydrophobic plug (Lorenz *et al*, 1993) (see below), as well as with the bottom of protomer B-1, including the C-terminus and the bottom of subdomain-3 (Figure 4A and B and Table I). Part of the main body of CP binds to the inner surface of protomer B. The interface of CP (Figure 4E) bears a cluster of basic residues, which are complementary to a cluster of acidic residues on the interface of the actin protomers (Figure 4C), and thus electrostatic interactions between these two clusters likely play major roles in the interaction.

In our fitted atomic model, the hydrophobic plug (Lorenz *et al*, 1993) of protomer B collides with the α-tentacle. No solid evidence was presented for the configuration of the
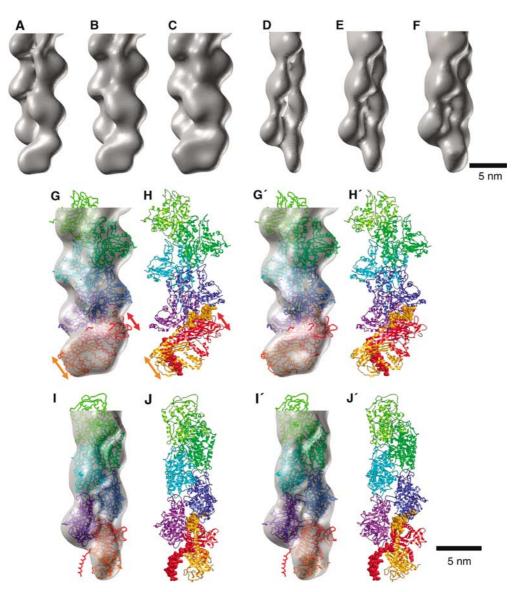
hydrophobic plug in Lorenz's model (Lorenz *et al*, 1993), which substantially differs from that in the crystal structures of monomeric actin (Kabsch *et al*, 1990; McLaughlin *et al*, 1993; Schutt *et al*, 1993). Moreover, the shape of the hydrophobic plug may differ at the barbed-end, since no other protomer below interacts with the plug. The α-tentacle may also change its conformation, since its temperature factor is relatively high (Yamashita *et al*, 2003). In addition, the C-terminal region and the hydrophobic plug of actin might be flexible, even in the middle of the actin filament (Kim *et al*, 2000; Yasunaga and Wakabayashi, 2001). Therefore, it is plausible that both sides of the interface undergo some conformational changes upon binding. For example, Glu270 on the hydrophobic plug is included in the acidic cluster (Table I) in our current model, and may form an important salt bridge with a basic residue on CP upon conformational change.

### Mutational analyses

Our interpretation that the CP–actin interactions through the α-tentacle are primarily electrostatic was confirmed by the mutation experiments. Three highly conserved basic residues in the α-tentacle (Figures 4D and 5) were replaced; R260 and R266 are within the interface (Table I), whereas K256 is very close to the interface. We performed elongation assays of the actin filament (Figure 6). CP inhibits the elongation, while triple mutants (KRR256 260 266EEE and KRR256 260 266AAA) showed dramatically impaired inhibitory activity. Double mutants with inverted charges (KR256 260EE, KR256 266EE and RR260 266EE) were more effective than double mutants replaced by alanines (KR256 260AA, KR256 266AA and RR260 266AA). Single mutants with an inverted charge (K256E, R260E and R266E) were also more effective than single mutants with alanine (K256A, R260A and R266A), although the effect of the single mutants was limited. These results are consistent with our interpretation.

Our fitted model also predicted that E200(α) (Figure 4E), which is not on either tentacle but on the surface of the main body of CP, may also contribute to the CP–actin interaction, since E200(α) can form a salt bridge with either K284 or R290 on actin protomer B (Figure 4C). Our actin filament elongation tests indicated that E200R reduced the inhibitory activity of CP more than E200A did (Figure 6). This may indicate that the interactions of CP–actin was suppressed either by an electrostatic effect of the reversed charge of E200R(α). Or the result may be explained in terms of steric hindrance of the side chain of Arg that is bulkier than that of Glu. In either case, the result indicates that E200 contributes to the interaction of CP to the actin filament. This is consistent with our docking model, and also with previous results obtained from the yeast cell (Sizonenko *et al*, 1996).

The electrostatic binding of CP described here represents a novel manner of binding between an actin binding protein and actin. No complex structure is known in which an actin binding protein binds to the inner surface (the surface that faces the filament axis) of the actin protomer (Dominguez, 2004; Aguda *et al*, 2005). Some small peptides like phalloidin (Oda *et al*, 2005) and dolastatin-11 (Oda *et al*, 2003), which stabilize actin filaments, bind to the inner surface. However, they lack charged groups.

**Figure 3** The 3D structure of the CP–actin complex obtained by cryo-electron microscopy was fitted with atomic models. (A–F) The 3D electron density map of the actin–CP complex presented at the contour level that envelops 70% (**A, D**), 100% (**B, E**) and 150% (**C, F**) of the calculated volume, respectively. The viewing angle is different by 90° between (A–C) and (D–F). (**G, H/G′, H′**) The atomic structures of CP (Yamashita *et al*, 2003) and of an actin filament (Lorenz *et al*, 1993) (H/H′) were fitted to and superposed on the 3D density map (G/G′) and displayed as stereo pairs. (**I, J/I′, J′**) Same as above, but viewed from the left-hand side of the above. In (G, H/G′, H′) and (I, J/I′, J′), individual actin protomers are colored light green, green, cyan, blue and purple, respectively, while the α- and β-subunits of CP are orange and red, respectively. In (H/H′) and (J/J′), the α- and β-tentacles of CP are presented in space filling models in orange and red, respectively. In (G) and (H), the orange and red arrows indicate the widths of the left and right edges of CP in the orientation in (G), respectively, in the 3D density map.

### Construction of a plausible model for the β-tentacle bound to the actin filament

In contrast to the α-tentacle, the mass assignable to the β-tentacle was not clearly distinguished in our 3D density map (Figure 3I). We propose that the β-tentacle likely interacts with the hydrophobic cleft between subdomains 1 and 3 of actin protomer B, as indicated in Figure 7H and I, because of the following four reasons. First, in the crystal structure (Yamashita *et al*, 2003), the basal part of the β-tentacle (residues 246–252) forms an extended loop that must be flexible (Figure 7H), and no part of the β-tentacle interacts with the main body of CP. Therefore, the β-tentacle is most likely freely mobile. Second, in the crystal structure (Yamashita *et al*, 2003), the α-helix of the β-tentacle is amphipathic and the hydrophobic residues, such as L262

and L266, on the hydrophobic side are well conserved (Barron-Casella *et al*, 1995) and crucially important for the CP–actin binding (Barron-Casella *et al*, 1995; Wear *et al*, 2003). Third, as pointed out by Dominguez (2004), many actin-binding proteins interact with the hydrophobic cleft along the boundary between subdomains-1 and -3 of the actin protomer, which serves as the binding site for an amphipathic α-helix. Fourth, for this binding, either polarity is possible for the directional relationship between the cleft and the α-helix.

By taking these considerations into account, the β-tentacle bound to the actin protomer was modeled, based on the crystal structure of the actin monomer–ciboulot complex (Figure 7B) (Hertzog *et al*, 2004). The sequences of the actin-binding α-helix of the ciboulot peptide and the
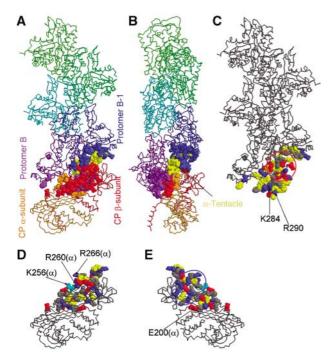
**Figure 4** The interface between actin and CP. The residues in the space-filling model include all of the residues at the interface (Table I), according to the criterion given in Materials and Methods. (**A, B**) The α- and β-subunits (α, orange and β, red) of CP, the bottom actin protomer (protomer B, purple) and the protomer directly above it (protomer B-1, blue) are presented as main chains. The α-tentacle is displayed in yellow. (B) The figure is rotated by 90° about the filament axis relative to (A). (**C**) The interface on the actin filament, showing a cluster of acidic residues as indicated by a red circle. (**D, E**) The interface on CP, viewed at two angles that differ by 180°. The blue circle in (E) indicates a cluster of basic residues. In (C–E), acidic, basic and hydrophobic residues are colored red, blue and yellow, respectively. K256(α), indicated in cyan in (D, E), is not involved in the interface, but lies at the edge of the interface. In (A), (C), (D), and in (B), the filament and/or CP are viewed in the same direction as in Figure 3H and J, respectively.

β-tentacle were aligned (Figure 7A) by aligning the repeated hydrophobic residues (in orange boxes), which form the hydrophobic surfaces of amphipathic α-helices. According to this sequence alignment, the two α-helixes were structurally aligned using ProFit (Martin ACR, http://www.bioinf.org.uk/software/profit). Then, the ciboulot peptide was replaced by the β-tentacle. We also replaced the structure of the monomeric actin in the ciboulot–actin complex (Figure 7B) by the actin protomer B in our atomic model for CP–actin (Figure 4A). The resultant model is presented in Figure 7C. In Figure 7H and I, this model is superposed on the atomic model of CP–actin. In the model, the β-tentacle is not extended into the solvent (in red), but lies (in black) on the actin protomer B, extending from the backside (the inner surface) to the front side (the outer surface) of protomer B. It is remarkable that, with this position and polarity, the base of the β-tentacle is located at almost an identical position as that in the CP–actin model. The β-tentacle placed on actin protomer B and the β-tentacle in the crystal structure fitted to the EM map are merged at about residues I-249 and P-250, which are within the flexible linker region. This indicates that a simple bend at the flexible basal part translocates the entire β-tentacle from the position found in the crystal structure

to the proposed position for the actin binding. The interacting surfaces on β-tentacle and actin are formed by hydrophobic residues (Figure 7E–G), indicating that hydrophobic interactions are predominant for β-tentacle binding to actin. A T-test calculation of the density map indicated that the density of the proposed β-tentacle binding surface on the actin protomer B was significantly higher than that of the equivalent region on other protomers (Figure 8). This provides another support for the proposed location of β-tentacle, although this is not a convincing evidence due to the limited resolution of the present density map.

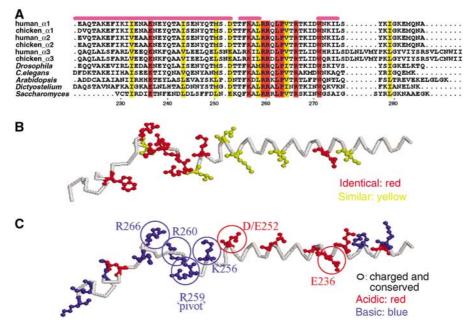## Discussions

### A new actin–CP binding model

Here we present a refined model for the binding of CP to the actin filament B-end (Figure 9). First, CP is attracted to the barbed-end of the actin filament through the electrostatic interactions between the basic residues, which are mainly but not exclusively on/around the α-tentacle (Figure 4E), and the acidic residues on the extreme surface at the barbed-end of the actin filament (Figure 4C). The electrostatic interactions through the α-tentacle may be the major determining factors of the on-rate of the binding. This is because that the deletion of the β-tentacle altered only the off-rate of the binding, without changing the on-rate (Wear et al, 2003). In contrast, the deletion of the α-tentacle reduced both the on- and off-rates (Wear et al, 2003). Second, the β-tentacle finds the hydrophobic binding site on the front surface of actin protomer B. This occurs because the β-tentacle is freely mobile at the flexible region in its base (around residues 246–252). The binding of the β-tentacle acts as a lock, and thus reduces the off-rate as suggested previously (Wear and Cooper, 2004). The proposed model dissects the binding into two elementary steps: the first step, through the interaction between the α-tentacle and the two end protomers, is of an electrostatic nature, which determines the on-rate, while the second step, through the interaction between the β-tentacle and one end protomer, is of a hydrophobic nature, which determines the off-rate.

This two-step binding mechanism implies that the binding is possible even without the β-tentacle. This is because the first step alone fulfills two requirements for the barbed-end capping: the recognition of the barbed-end and the inhibition of polymerization and depolymerization. First, the cluster of acidic residues is exposed only at the barbed end, not in the middle or at the pointed end of the filament, so that the barbed-end is easily recognized by the positively charged region on CP, including the α-tentacle. Second, the binding of CP after the first step covers the surface of both protomers B and B-1, and thereby prevents the binding of a new actin monomer as well as the detachment of the end protomers. The idea that the capping activity can persist even without the β-tentacle is entirely consistent with the previous experimental results (Kim et al, 2004; Wear et al, 2003). The deletion of the α-tentacle weakens the affinity of CP–actin by 5000-fold, whereas the deletion of the β-tentacle impaired the affinity by only between six- and 400-fold. Moreover, the deletion of the β-tentacle did not impair the growth rate of the cell, the localization patterns of CP, and the amount of CP at the actin patches in the yeast cell (Kim et al, 2004).

**Table I** Residues at the interface between CP and the actin filament end

(A)

| Molecule | The residues at the interface |
| --- | --- |
| Actin (B) | L110, K113, G168–D179, E195, E224, M227, E259, F262–G273, H275–T277, Y279–I287, R290, R312, K315, E316, T318–P322, M325, F375 |
| Actin (B-1) | R116, Y133, V134, I136, V139, Y143, T148, T149, I165–A170, D286–D288, T351, F352, Q354, M355, H371–F375 |
| CP (α) | Y198, E200, D201, S244, Q248, S251, D252, R260–R270, N272–I274, S276–G280, K281 |
| CP (β) | N102, D105, Q106, D109, L110, E113, R195–M197, K199, R215, D219, N222–I224, S226, T227, N229–I231, F233–K235, K237, D238, N241, D247 |

(B)

| Molecule | The residues in the acidic cluster |
| --- | --- |
| Actin (B) | D179, E224, E259, E270, E276, E316 |
| Actin (B-1) | E167, D286, D288 |

| Molecule | The residues in the basic cluster |
| --- | --- |
| CP (α) | R260, R266, K268 |
| CP (β) | R195, K199, R215, K223 |

(C)

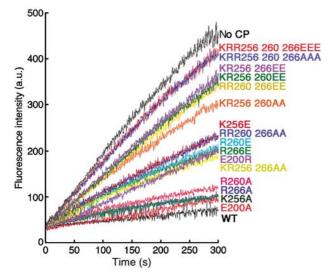| Molecule | The residues at the interface |
| --- | --- |
| Actin (B) | Y143, A144, S145, G146, I345, L346, L349, S350, T351, Q354, M355 |
| CP (β) | L258, L262, S263, V265, L266, T267, R269, Q270, I271 |

(A) A list of all the residues within the CP–actin interface of the 3D electron density map obtained in the present study (indicated in the space filling model in Figure 4). (B) A list of the residues (a subgroup of the residues listed in A) included in the acidic cluster (Figure 4C) on the end actin protomers, and in the basic cluster on CP (Figure 4E). (C) A list of the residues on the interface between the β-tentacle and the end actin protomer (shown in the space filling model in Figure 7D–G). Any residue with one or more atoms that have van der Waals contact with any other atom of the other molecule in the model in Figure 7C was identified as a residue at the interface between the actin protomer and the β-tentacle.



**Figure 5** Conserved residues at the C-terminal region of the CP α-subunit. (**A**) A sequence alignment of the C-terminal region of the CP α-subunit. The C-terminal region sequences of human α1 (GenBank Accession Number U56637), chicken α1 (M25534), human α2 (U03269), chicken α2 (M80589), human α3 (BC016745), chicken α3 (XM 425501), *Drosophila* α (NM 137695), *Caenorhabditis elegans* α (NM 068744), *Arabidopsis* α (AJ001855), *Dictyostelium* α (XM 640151) and *Saccharomyces* α (X61398) are aligned, and the strictly and moderately conserved residues are highlighted in red and yellow, respectively. The magenta bar indicates α-helix forming residues. The residue numbers corresponding to chicken α1 are indicated at the bottom. (**B, C**) The residues at the C-terminal region of the CP α-subunit (helix 5 and downstream) are illustrated. The N-terminus is located on the right-hand side. (B) The strictly and moderately conserved residues indicated in (A) are shown in ball-and-stick model and colored red and yellow, respectively. (C) The side chains of the charged residues are indicated in ball-and-stick model, in red for acidic residues and blue for basic residues, and the conserved residues indicated in (A) are circled. Since K256, K260, and R266 are basic, highly conserved, and exposed on the surface of CP, we selected these residues as mutagenesis targets. R259 is also a basic and conserved residue, but it is buried deep in the core of CP, where it forms multiple salt bridges with other residues, suggesting that the side chain of R259 forms a stable anchorage point ('pivot') of the α-tentacle to the body of CP (Yamashita *et al*, 2003). The capping activity of the R259 mutant was examined previously (Wear *et al*, 2003).

It is also worth noting that the electrostatic interactions are advantageous for the first step of the CP–actin binding. The electrostatic interactions between two clusters of homogenously charged residues like the interaction between CP and actin in our model do not require precise fitting between two surfaces to dock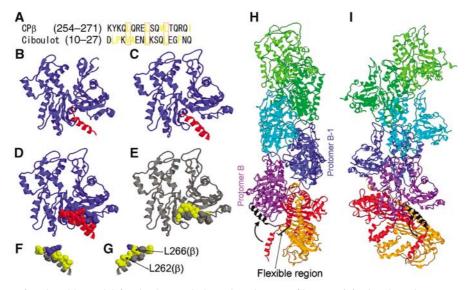. The actin filament barbed-end may be dynamic, especially considering the fluctuation of the lateral separation between the two strands, and therefore between protomers B and B-1 (T Oda and Y Maéda, unpublished results). The electrostatic interactions of CP with both protomers at the end provide a connection between the two protomers. Thus, CP stabilizes the barbed-end, even with its fluctuations.

This is the first structural determination of the end of an actin filament. The actin filament end is particularly important for our understanding of actin filament dynamics, because polymerization and depolymerization occur only at the end. Our newly established image analysis procedures (Narita and Maéda, 2006), which were developed for the present study, are also applicable to the actin filament end structure in complex with formin, gelsolin, the Arp2/3 complex, and tropomodulin (reviewed in Fischer and Fowler, 2003; Pollard and Borisy, 2003; Zigmond, 2004). These structures would let us know the mechanism by which the end-binding proteins regulate actin filament dynamics.
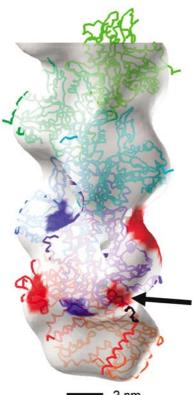


**Figure 6** Actin filament elongation assays by the use of various CP mutants. Elongation of the actin filament (1 μM, 5% pyrene labeled) from prepolymerized actin filaments (1.25 μM) in the presence of 5 μM CP mutant proteins was measured as the time course (in s) of pyrene fluorescence intensity (in arbitrary units, a.u.) WT, wild-type CP. The pyrene fluorescence intensity increases in proportion to the amount of actin protomers incorporated in the filament.

## Materials and methods

### Proteins

The chicken muscle CapZα1 and β1 (CP in muscle is referred to as CapZ) subunits were co-expressed in *Escherichia coli* BL21 (DE3) pLys-S (Novagen) and were purified as described (Soeno *et al*, 1998; Yamashita *et al*, 2003). The bacterial expression vectors for the mutant CP constructs (His6-tagged at the N-terminus of the β-subunit) were created in the pETDuet vector (Novagen) by PCR, using pET-3d/CP (Soeno *et al*, 1998) as a template and mutations were introduced by QuikChange Site-Directed Mutagenesis Kit (Stratagene). CP variants were expressed in *E. coli* BL21 (DE3) and were purified using Ni-NTA Superflow (Qiagen). Actin was



**Figure 7** Construction of a plausible model for the β-tentacle bound to the actin filament. (**A**) The aligned sequences of the β-tentacle of chicken muscle CP (Caldwell *et al*, 1989b) and the actin binding α-helix of ciboulot (Hertzog *et al*, 2004). (**B**) Crystal structure of the actin–ciboulot complex (Hertzog *et al*, 2004). The monomeric actin is in a blue ribbon model, while residues 10–27 of ciboulot are red. (**C**) The α-helix of ciboulot in B was replaced by a part of the β-tentacle (254–271) (red) of the crystal structure (Yamashita *et al*, 2003) of CP, and the actin monomer in (B) was replaced by one actin protomer (blue) within the F-actin model (Lorenz *et al*, 1993). In (**D–G**), all of the residues expected to comprise the interface are presented in a space-filling model (for the assigned residues and the criterion for the assignment, see Table IC and the legend thereof). (**D**) The interface residues of each molecule are indicated, using the same color-code as in (C). (**E**) The interface residues on the actin protomer. (**F**) The interface residues on the β-tentacle. (**G**) As in (F), but after a rotation by 180° about the filament axis. In (E–G) acidic, basic and hydrophobic residues are red, blue and yellow, respectively. (**H**) A plausible conformational change of the β-tentacle upon its binding to the end actin protomer. This is identical to Figure 3J, except that the β-tentacle, in black, is now in the proposed position on the protomer B as indicated in (C). (**I**) The same as (H) but viewed from a direction that is by 90° different from (H).

2 nm

**Figure 8** Differences in density distribution between the end protomer and the other protomers. The results of the *T*-test between actin protomers are indicated on the 3D density map that is related to Figure 3C by a 180° rotation. The regions colored red and blue are where the density of the actin protomer was higher or lower, respectively, than that of the rest by 97% probability. The β-tentacle in the proposed position (Figure 7H and I, in black) is superposed and indicated by a black arrow. Around the proposed β-tentacle position was colored red, in spite of that the mass of β-tentacle is small. This is consistent with our binding model of the β-tentacle to actin protomer B.
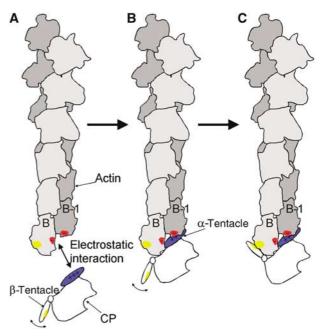
prepared from rabbit skeletal muscle, as previously described (Spudich and Watt, 1971). For polymerization assay, actin was labeled with pyrenyliodoacetamide as described (Kouyama and Mihashi, 1981).

### Actin filament elongation assay

Barbed-end elongation assay was performed essentially as described (Harris *et al*, 2004). Briefly, 1.25 μM phalloidin-stabilized actin filaments and 5 μM CP were premixed in a solution containing 100 mM KCl, 2 mM $MgCl_2$, 2 mM EGTA, 20 mM imidazole buffer, pH 7.0 (2 × conc. polymerization buffer). Polymerization was initiated by mixing the above-indicated solution of actin fragments with an equal volume of the solution that contains 2 μM G-actin (10% pyrene-labeled) and 5 μM CP, in $Mg^{2+}$-converted G buffer (1 mM $MgCl_2$, 0.2 mM $CaCl_2$, 1 mM EGTA, 0.2 mM ATP, 0.5 mM DTT, 10 mM imidazole buffer, pH 7.0). Pyrene fluorescence (excitation 368 nm, emission 388 nm) was monitored at 25°C.

### Cryo-electron microscopy

Actin (0.5 mg/ml) and CP (0.011 mg/ml: at a molar ratio of 70:1) were mixed and incubated for 45 min at 25°C, in the solution containing 50 mM NaCl, 10 mM sodium phosphate buffer (pH 7.4), 3 mM $MgCl_2$, 0.005% (w/v) $NaN_3$, and 0.7 mM DTT. Extra CP (0.0075 mg/ml) was then added to ensure that all of the actin filament ends were capped. The solution was diluted by the same solution except protein just before the application to the grid. The grid was rapidly frozen by plunging into liquid ethane. The images of the ice-embedded actin–CP complexes were recorded on Kodak



**Figure 9** A proposed model for the binding of CP to the actin filament barbed-end. (**A**) First, the basic residues on the α-tentacle (blue) and the acidic residues on the bottom of the actin filament (red) attract each other. This interaction should determine the on-rate of the binding. The unbound β-tentacle (yellow) is freely mobile, due to the flexibility at the basal part (around residues 246–252). (**B**) Second, the α-tentacle binds to the bottom of the actin filament. The β-tentacle remains freely mobile, and searches for its binding position on the actin filament. (**C**) The β-tentacle binds to the hydrophobic cleft (yellow) on the outer surface of the end protomer B. This binding reduces the off-rate of the binding, and thereby stabilizes the binding.

SO163 photographic film with 5–8 μm defocuses at a magnification of 40 000 at 300 kV (34 electron/$Å^2$ dose), using a liquid helium stage in a JEOL JEM300-EFC electron microscope equipped with an energy filter. The films were digitized with a PhotoScan2000 scanner (Z/I Imaging) at 7 μm steps (1 pixel = 1.75 Å). Then the images were shrunk and adjusted so that the final pixel size was 3.4125 Å.

### Image analysis

The image analysis was performed by employing our newly established procedures, which were specially designed for single particle analysis of the end structures of the actin filament (Narita and Maéda, 2006).

Additional refinement steps were performed on the obtained structure. First, we calculated the Fourier Shell Phase Residual (FSPR) (van Heel, 1987) between the projections of the obtained 3D density map and each image on the electron micrographs in two resolution ranges, one between 270 and 42 Å and the other between 42 and 22 Å. Those images with FSPR values larger than 60° in the first range and those with FSPR values larger than 85° in the second range were discarded. From the remaining images, a three-dimensional structure was reconstructed. The first and the second ranges were chosen so that the resolution of the reconstructed structure from the selected images was significantly improved. Second, the azimuth angles of the remaining images were refined using only the region near the end (within the axial period of 136.5 Å). Then, the final resolution was evaluated by Fourier Shell Correlation (van Heel, 1987).

All of the image analysis was performed on Eos (Yasunaga and Wakabayashi, 1996). The final 3D electron density map was obtained from 876 images. The final map in Figure 3 was presented after passed through a median filter (kernel radius = 5.1 Å) followed by a low-pass filter (23 Å), to reduce the noise.

### Residues at the interface

The F-actin atomic model (Lorenz *et al*, 1993) was fitted to the final map (before being filtered) by using pdbRhoFit on Eos. The mass associated with the pixels within 3.5 Å from any of the atoms of the fitted model was removed. The remaining volume due to CP was passed through a median filter (kernel radius = 5.1 Å) followed by a low-pass filter (23 Å), to reduce the noise. To the resultant volume, the atomic structure of CP (Yamashita *et al*, 2003) was fitted by Situs (Wriggers and Birmanns, 2001). Actin residues with one or more atoms within 6 Å from the 140% volume contour of the resultant CP map were assigned as interface residues (Figure 4A–C). To assign the CP residues at the interface (Figure 4A, B, D and E), the reverse procedures were performed; from the final 3D density map, the mass associated with the fitted CP atomic model was removed, and the resultant actin filament map was passed through the same filter. CP residues with atoms within 6 Å from the 140% volume contour of the resultant actin filament map were assigned as CP residues at the interface.

### T-test calculation between actin protomers

All the 876 filament images used in the final reconstruction were divided into three groups and, from images of each group, one structure was reconstructed. From each of the three reconstructed structures, actin protomers were extracted one by one from the end actin protomer (protomer B) followed by next 19 protomers. In order to know differences in the density distribution of actin protomers at the end relative to the next 19, *T*-values were calculated, first between three structures of protomer B and the remaining 57 ( = 3 × 19) extracted structures, followed by between three B-1 protomers and the remaining 57, and so on.

## Acknowledgements

## References

Aguda AH, Burtnick LD, Robinson RC (2005) The state of the filament. *EMBO Rep* **6:** 220–226

Barron-Casella EA, Torres MA, Scherer SW, Heng HH, Tsui LC, Casella JF (1995) Sequence analysis and chromosomal localization of human Cap Z. Conserved residues within the actin-binding domain may link Cap Z to gelsolin/severin and profilin protein families. *J Biol Chem* **270:** 21472–21479

Caldwell JE, Heiss SG, Mermall V, Cooper JA (1989a) Effects of CapZ, an actin capping protein of muscle, on the polymerization of actin. *Biochemistry* **28:** 8506–8514

Caldwell JE, Waddle JA, Cooper JA, Hollands JA, Casella SJ, Casella JF (1989b) cDNAs encoding the beta subunit of cap Z, the actin–capping protein of the Z line of muscle. *J Biol Chem* **264:** 12648–12652

Casella JF, Craig SW, Maack DJ, Brown AE (1987) Cap Z(36/32), a barbed end actin–capping protein, is a component of the Z-line of skeletal muscle. *J Cell Biol* **105:** 371–379

Dominguez R (2004) Actin-binding proteins—a unifying hypothesis. *Trends Biochem Sci* **29:** 572–578

Fischer RS, Fowler VM (2003) Tropomodulins: life at the slow end. *Trends Cell Biol* **13:** 593–601

Frank J (2002) Single-particle imaging of macromolecules by cryo-electron microscopy. *Annu Rev Biophys Biomol Struct* **31:** 303–319

Harris ES, Li F, Higgs HN (2004) The mouse formin, FRLalpha, slows actin filament barbed end elongation, competes with capping protein, accelerates polymerization from monomers, and severs filaments. *J Biol Chem* **279:** 20076–20087

Hertzog M, van Heijenoort C, Didry D, Gaudier M, Coutant J, Gigant B, Didelot G, Preat T, Knossow M, Guittet E, Carlier MF (2004) The beta-thymosin/WH2 domain; structural basis for the switch from inhibition to promotion of actin assembly. *Cell* **117:** 611–623

Isenberg G, Aebi U, Pollard TD (1980) An actin-binding protein from Acanthamoeba regulates actin filament polymerization and interactions. *Nature* **288:** 455–459

Kabsch W, Mannherz HG, Suck D, Pai EF, Holmes KC (1990) Atomic structure of the actin:DNase I complex. *Nature* **347:** 37–44

Kim E, Wriggers W, Phillips M, Kokabi K, Rubenstein PA, Reisler E (2000) Cross-linking constraints on F-actin structure. *J Mol Biol* **299:** 421–429

Kim K, Yamashita A, Wear MA, Maéda Y, Cooper JA (2004) Capping protein binding to actin in yeast: biochemical mechanism and physiological relevance. *J Cell Biol* **164:** 567–580

Kouyama T, Mihashi K (1981) Fluorimetry study of *N*-(1-pyrenyl) iodoacetamide-labelled F-actin. Local structural change of actin protomer both on polymerization and on binding of heavy meromyosin. *Eur J Biochem* **114:** 33–38

Loisel TP, Boujemaa R, Pantaloni D, Carlier MF (1999) Reconstitution of actin-based motility of Listeria and Shigella using pure proteins. *Nature* **401:** 613–616

Lorenz M, Popp D, Holmes KC (1993) Refinement of the F-actin model against X-ray fiber diffraction data by the use of a directed mutation algorithm. *J Mol Biol* **234:** 826–836

McLaughlin PJ, Gooch JT, Mannherz HG, Weeds AG (1993) Structure of gelsolin segment 1-actin complex and the mechanism of filament severing. *Nature* **364:** 685–692

Narita A, Maéda Y (2006) Molecular determination by electron microscopy of the actin filament end structure. *J Mol Biol*, in press

Oda T, Crane ZD, Dicus CW, Sufi BA, Bates RB (2003) Dolastatin 11 connects two long-pitch strands in F-actin to stabilize microfilaments. *J Mol Biol* **328:** 319–324

Oda T, Namba K, Maéda Y (2005) Position and orientation of phalloidin in F-actin determined by X-ray fiber diffraction analysis. *Biophys J* **88:** 2727–2736

Pantaloni D, Le Clainche C, Carlier MF (2001) Mechanism of actin-based motility. *Science* **292:** 1502–1506

Pollard TD, Borisy GG (2003) Cellular motility driven by assembly and disassembly of actin filaments. *Cell* **112:** 453–465

Schafer DA, Waddle JA, Cooper JA (1993) Localization of CapZ during myofibrillogenesis in cultured chicken muscle. *Cell Motil Cytoskeleton* **25:** 317–335

Schutt CE, Myslik JC, Rozycki MD, Goonesekere NC, Lindberg U (1993) The structure of crystalline profilin-beta-actin. *Nature* **365:** 810–816

Sizonenko GI, Karpova TS, Gattermeir DJ, Cooper JA (1996) Mutational analysis of capping protein function in *Saccharomyces cerevisiae*. *Mol Biol Cell* **7:** 1–15

Soeno Y, Abe H, Kimura S, Maruyama K, Obinata T (1998) Generation of functional beta-actinin (CapZ) in an *E. coli* expression system. *J Muscle Res Cell Motil* **19:** 639–646

Spudich JA, Watt S (1971) The regulation of rabbit skeletal muscle contraction. I. Biochemical studies of the interaction of the tropomyosin–troponin complex with actin and the proteolytic fragments of myosin. *J Biol Chem* **246:** 4866–4871

van Heel M (1987) Similarity measures between images. *Ultramicroscopy* **21:** 95–100

Wear MA, Cooper JA (2004) Capping protein: new insights into mechanism and regulation. *Trends Biochem Sci* **29:** 418–428

Wear MA, Yamashita A, Kim K, Maéda Y, Cooper JA (2003) How capping protein binds the barbed end of the actin filament. *Curr Biol* **13:** 1531–1537

Wriggers W, Birmanns S (2001) Using situs for flexible and rigid-body fitting of multiresolution single-molecule data. *J Struct Biol* **133:** 193–202

Yamashita A, Maeda K, Maéda Y (2003) Crystal structure of CapZ: structural basis for actin filament barbed end capping. *EMBO J* **22:** 1529–1538

Yasunaga T, Wakabayashi T (1996) Extensible and object-oriented system Eos supplies a new environment for image analysis of electron micrographs of macromolecules. *J Struct Biol* **116:** 155–160

Yasunaga T, Wakabayashi T (2001) Relocation of Cys374 of actin induced by labeling with fluorescent dyes. *J Biochem (Tokyo)* **129:** 201–204

Zigmond SH (2004) Beginning and ending an actin filament: control at the barbed end. *Curr Top Dev Biol* **63:** 145–188